Journal of Alloys and Compounds 502 (2010) 461–465

Contents lists available at ScienceDirect

Journal of Alloys and Compounds

journal homepage: www.elsevier.com/locate/jallcom

Effects of TiC addition on formation of Ti_2SnC by self-propagating combustion of Ti–Sn–C–TiC powder compacts

C.L. Yeh*, C.W. Kuo

Department of Aerospace and Systems Engineering, Feng Chia University, 100 Wenhwa Road, Seatwen, Taichung 40724, Taiwan

ARTICLE INFO

Article history:
Received 19 March 2010
Accepted 27 April 2010
Available online 5 May 2010

Keywords:
Ceramics
X-ray diffraction
SEM
Ti_2SnC
Combustion synthesis

ABSTRACT

Preparation of the ternary carbide Ti_2SnC was conducted by combustion synthesis in the mode of self-propagating high-temperature synthesis (SHS) using both the elemental powder compacts and TiC-added samples with TiC contents from 2.6 to 17.6 mol%. On account of the dilution effect of TiC on combustion, the reaction exothermicity was reduced by adopting TiC in the reactant mixture. As a result, the combustion temperature and reaction front velocity decreased significantly with increasing TiC content. Moreover, the self-sustaining combustion front was no longer planar and was confined to localized reaction zones in the samples with high proportions of TiC like 14.3 and 17.6 mol%. On the other hand, the yield of Ti_2SnC was substantially enhanced by the TiC-containing sample. For the elemental powder compact, the final product contains more Ti_6Sn_5 than Ti_2SnC, implying an incomplete phase conversion. In contrast, Ti_2SnC dominates in the products synthesized from the TiC-added samples and increases with TiC content, which is attributed to the prolonged reaction time and appropriate reaction temperature provided by the Ti–Sn–C–TiC powder compacts. The morphology of as-synthesized Ti_2SnC grains is also affected by the addition of TiC in the reactant mixture. The growth of rod-like Ti_2SnC grains was prevailing in the final product of the Ti–Sn–C powder compact, but the TiC-added samples favored the evolution of Ti_2SnC with a plate-like microstructure.

1. Introduction

Layered ternary compounds $M_{n+1}AX_n$, where $n = 1$, 2, or 3, M is an early transition metal, A is an A-group (mostly IIIA and IVA) element, and X is either C or N, are a new class of materials which combine many merits of both metals and ceramics [1,2]. Titanium tin carbide (Ti_2SnC) belonging to the M_2AX ($n = 1$) family, the so-called H-phase compound, was first identified by Jeitschko et al. [3]. Like other M_2AX carbides, Ti_2SnC exhibits a number of remarkable properties, such as low hardness, high electric conductivity, high modulus, and low thermal expansion coefficient [4–6]. In particular, Ti_2SnC possesses the highest electric conductivity among various Sn-containing carbides (M_2SnC, with M = Ti, Hf, Nb, and Zr) [4]. Moreover, Ti_2SnC is readily machinable, highly tolerant to damage, and resistant to corrosion; therefore, it has been considered as a promising reinforcement for metals and an attractive material for the electronic contact film [4–7].

Several processing routes, including hot isostatic pressing (HIP) [4,5], hot pressing (HP) [6–8], and pressureless sintering [9–13] have been adopted to prepare Ti_2SnC. In general, the synthesized Ti_2SnC from most of the previous studies was accompanied by small amounts of TiC, Ti_6Sn_5, and Sn. Barsoum et al. [4] first fabricated polycrystalline Ti_2SnC by HIP from a stoichiometric mixture of Ti, Sn, and graphite powders of at 1325 °C and 50 MPa for 4 h, and characterized its properties. El-Raghy et al. [5] further optimized the processing parameters of HIP and obtained Ti_2SnC at 1250 °C for 12 h. By an in situ solid-liquid reaction/hot pressing method, Zhou and co-workers [6–8] prepared bulk Ti_2SnC from elemental powder mixtures and proposed that Ti_2SnC was yielded through the reaction of TiC_x with Ti–Sn intermetallics at about 1100 °C. To develop composite materials reinforced by the carbide-coated carbon fibers, Vincent et al. [9] produced Ti_2SnC by conducting the chemical interaction between carbon and titanium dissolved in liquid tin and established the isothermal section of the Ti–Sn–C phase diagram at 1200 °C. The solid-liquid reaction in the Ti–Sn–C system was also performed by Dong et al. [10] to synthesize Ti_2SnC powders. Recently, Li et al. [11,12] employed the pressureless sintering technique to fabricate high-purity Ti_2SnC powders from the Ti–Sn–C and Ti–Sn–TiC powder mixtures at 1200 °C for 15–60 min in vacuum, and the as-synthesized Ti_2SnC grains with either plate- or rod-like shapes were observed. In addition, Li et al. [13] indicated the formation of Ti_2SnC at a relatively low temperature of 650 °C when the reactant powders were pretreated by mechanical activation.

* Corresponding author. Tel.: +886 4 24517250x3963; fax: +886 4 24510862.
E-mail address: clyeh@fcu.edu.tw (C.L. Yeh).

0925-8388/$ – see front matter © 2010 Elsevier B.V. All rights reserved.
doi:10.1016/j.jallcom.2010.04.196

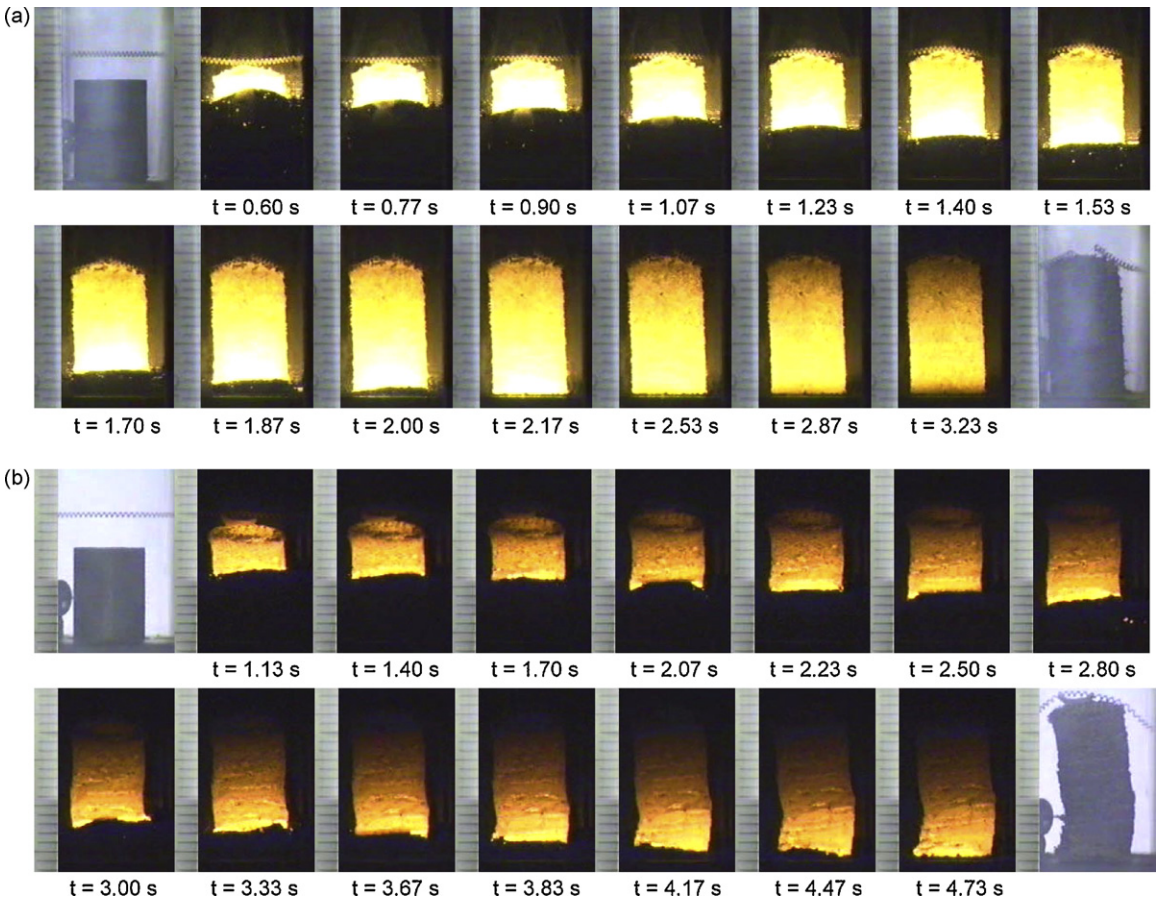

Fig. 1. Typical SHS sequences recorded from solid state combustion of TiC-containing powder compacts of $(2-x)$Ti + Sn + $(1-x)$C + xTiC with (a) $x = 0.2$ and (b) $x = 0.5$.

When compared with the above-mentioned methods, combustion synthesis in the mode of self-propagating high-temperature synthesis (SHS) takes advantage of the self-sustaining merit from highly exothermic reactions and hence has the benefits of low energy requirement, short reaction time, and simple facilities [14–16]. Moreover, the SHS technique has been effectively applied to produce a number of the MAX carbides, like Ti_3SiC_2 [17,18], Ti_3AlC_2 [19,20], Ti_2AlC [21,22], Ta_2AlC [23], and Nb_2AlC [24]. As the first attempt, this study aims at the synthesis of Ti_2SnC by solid state combustion in the mode of SHS with the green samples compressed from both the Ti–Sn–C and Ti–Sn–C–TiC powder mixtures. Effects of the content of TiC in the reactant compact are studied on the phase composition and morphology of the synthesized product, as well as on the reaction temperature and propagation velocity of the combustion front. In addition, the reaction mechanism is investigated for formation of Ti_2SnC through self-sustaining combustion.

2. Experimental methods of approach

Titanium (Strem Chemicals, <45 μm, 99% purity), tin (Strem Chemicals, <45 μm, 99.8% purity), carbon black (Showa Chemical Co.), and titanium carbide TiC (Aldrich Chemical, <45 μm, 98% purity) powders were used as the starting materials. Test samples of two different types were conducted in this study. One was prepared from the elemental powder mixture of Ti, Sn, and carbon at Ti:Sn:C = 2:1:1. The other contains TiC powders in addition to Ti, Sn, and carbon. For the TiC-containing samples, the reactant powders were formulated with an atomic ratio of Ti:Sn:C = 2:1:1, as expressed in the following reaction:

$$(2-x)\mathrm{Ti} + \mathrm{Sn} + (1-x)\mathrm{C} + x\mathrm{TiC} \rightarrow \mathrm{Ti_2SnC} \quad (1)$$

where the stoichiometric parameter x varies from 0.1 to 0.6, signifying the content of TiC in the Ti–Sn–C–TiC mixture ranging between 2.6 and 17.6 mol%. The reactant powders were dry mixed in a ball mill and then cold-pressed into cylindrical samples with a diameter of 7 mm, a height of 12 mm, and a compaction density of 60% relative to the theoretical maximum density (TMD).

The SHS experiments were performed in a stainless-steel windowed combustion chamber under an atmosphere of high-purity argon (99.99%). Details of the experimental setup and measurement approach were reported elsewhere [25,26]. The microstructure of synthesized products was examined under a scanning electron microscope (Hitachi S-3000N), and phase composition was analyzed by an X-ray diffractometer (Shimadzu XRD-6000) with CuK_α radiation.

3. Results and discussion

3.1. Observation of combustion characteristics

Two typical combustion sequences illustrated in Fig. 1(a) and (b) are related with two different propagation modes of the combustion wave observed in this study. For the elemental powder compact and TiC-added samples with TiC up to about 11 mol% ($x \leq 0.4$), as shown in Fig. 1(a), the SHS process is characterized by a nearly planar combustion front traversing the entire sample in a self-sustaining manner. As the content of TiC in the green sample increases and reaches 14.3 mol% ($x = 0.5$), Fig. 1(b) indicates that the reaction front is no longer planar and is confined to a couple of localized regions moving along a spiral trajectory on the sample surface; thus, it took longer time of about 4.73 s for the combustion wave to arrive at the bottom of the sample than that revealed in Fig. 1(a). According to Ivleva and Merzhanov [27], once the heat flux liberated from self-sustaining combustion is insufficient to maintain steady propagation of a planar front, the reaction front forms one or several localized reaction zones. Such a change in the propagation mode of the combustion wave is attributed to the dilution effect of TiC on combustion of the Ti–Sn–C–TiC powder compact, because the reaction of Ti with carbon forming TiC is considered as the major heat releasing step to sustain combustion in either the

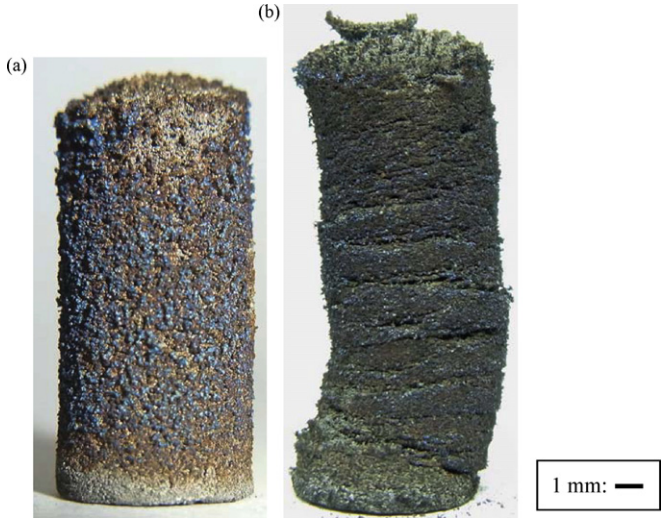

Fig. 2. Photographs of final products synthesized from TiC-containing powder compacts of $(2-x)$Ti + Sn + $(1-x)$C + xTiC with (a) $x = 0.2$ and (b) $x = 0.5$.

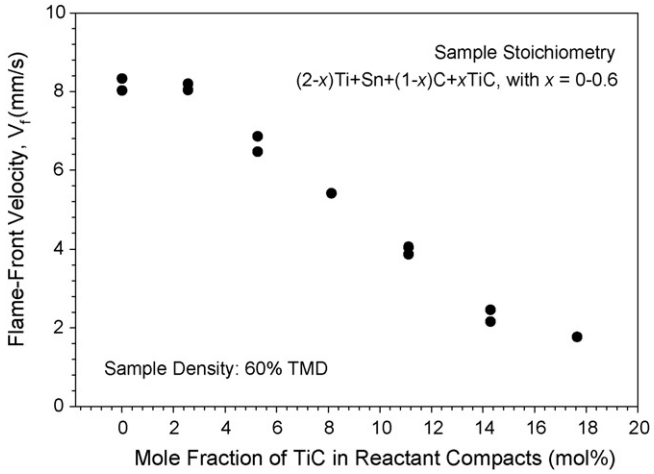

Fig. 3. Effect of TiC content on flame-front propagation velocity of Ti–Sn–C–TiC powder compacts.

Ti–Sn–C or Ti–Sn–C–TiC reaction system. Therefore, the increase of TiC in the Ti–Sn–C–TiC powder compact reduces exothermicity of the reaction. The spinning combustion wave was also observed in the sample with TiC of 17.6 mol% ($x = 0.6$), beyond which the reaction ceased to propagate and was quenched shortly after ignition due to lack of adequate reaction heat.

Furthermore, as illustrated in Fig. 1(a) and (b), during the progression of the combustion front the sample compacts were subjected to a considerable axial elongation and a slight radial contraction. Formation of elongated products has been reported in the preparation of many ternary carbides by combustion synthesis, including Ti_3SiC_2 [17,18], Ti_3AlC_2 [19,20] and Ti_2AlC [21,22]. It is believed that the axial elongation of the burned sample is most likely caused by the growth of Ti_2SnC grains into a terraced structure [28]. The radial contraction is due to the surface tension effect of the liquid melt formed in the reaction sequence [19–21]. The liquid phase substances present in the Ti–Sn–C(-TiC) combustion system could include molten Sn and Ti–Sn intermetallics.

Photographs of two final products synthesized from TiC-added powder compacts with TiC of 5.3 and 14.3 mol% ($x = 0.2$ and 0.5) are presented in Fig. 2(a) and (b), respectively. The recovered sample in Fig. 2(a) represents the typical product formed through propagation of a planar combustion front. For the reactant compact experiencing a spinning combustion wave, the burned sample with several trajectory marks left on the external surface is shown in Fig. 2(b). Consequently, the product of Fig. 2(b) tends to fracture into laminated pieces. It is of interest to note that there exist many agglomerated tiny particles with metallic glow on the product surface of Fig. 2(a). Those metallic compounds are composed largely of Ti and Sn. The presence of Ti–Sn granules might imply an incomplete phase conversion, because Ti–Sn intermetallics like Ti_6Sn_5 and Ti_5Sn_3 have been considered as the intermediates for formation of Ti_2SnC in the Ti–Sn–C (or -TiC) system [6,10–12].

3.2. Measurement of flame-front propagation velocity and combustion temperature

The flame-front propagation velocity (V_f) was determined from the combustion wave trajectory constructed upon the recorded film images. As depicted in Fig. 3, the flame-front velocity is substantially affected by the addition of TiC in the sample and decreases with increasing TiC content. Although the flame-front velocity of the 2.6 mol% TiC-added sample is comparable to that of the elemental powder compact, the increase of TiC addition from 2.6 to 17.6 mol% leads to a significant decrease in the flame velocity from 8.2 to 1.8 mm/s. The decrease of combustion velocity is attributed to the reduction of reaction exothermicity caused by the dilution effect of TiC. In addition to weaker exothermicity, the spiral propagation of the reaction zone is responsible for the low flame speeds observed in the samples with TiC of 14.3 and 17.6 mol%.

Fig. 4 plots measured temperature profiles from solid state combustion of the elemental powder compact and TiC-added samples with different TiC contents. As shown in Fig. 4, the abrupt rise in temperature signifies rapid arrival of the combustion front and the peak value corresponds to the combustion front temperature. After the passage of the combustion wave, an appreciable decrease in temperature is a consequence of heat losses to the surroundings. The flame-front temperatures varying from 1190 to 1650 °C are indicated in Fig. 4 and, more importantly, the composition dependence of combustion temperature is consistent with that of reaction front velocity. This confirms the dilution effect of TiC on solid state combustion of the Ti–Sn–C–TiC powder compacts. The reaction temperatures presented in Fig. 4 certainly melt elemental Sn, but molten Ti–Sn intermetallics (possible in the form of Ti_5Sn_3 and Ti_6Sn_5) exist only in the cases with a reaction temperature higher than their melting points of about 1500 °C [29].

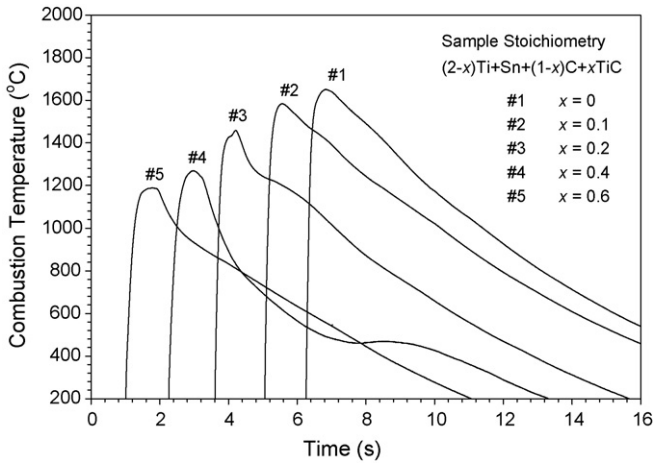

Fig. 4. Effect of TiC content on combustion temperature of Ti–Sn–C–TiC powder compacts.

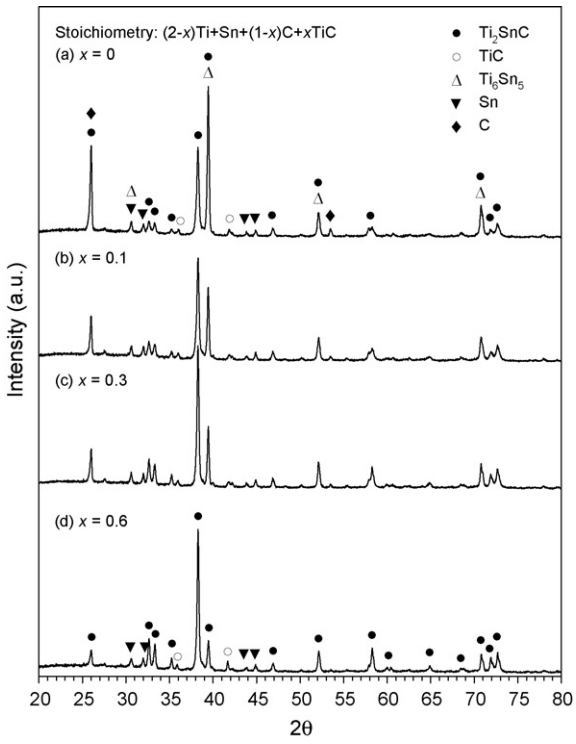

Fig. 5. XRD patterns of products synthesized from powder compacts of $(2-x)$Ti + Sn + $(1-x)$C + xTiC with (a) $x = 0$, (b) $x = 0.1$, (c) $x = 0.3$, and (d) $x = 0.6$.

3.3. Composition and morphology of combustion products

XRD patterns in Fig. 5 show the phase composition of the final products synthesized from reactants of different starting stoichiometries. Fig. 5(a) indicates that for the Ti–Sn–C powder compact the intermetallic Ti_6Sn_5 dominates over Ti_2SnC in the final product. Besides, TiC was identified as a secondary phase and some unreacted Sn and carbon were detected. For the Ti–Sn–C–TiC samples, however, Fig. 5(b)–(d) reveals that formation of Ti_2SnC is significantly enhanced and the content of Ti_2SnC formed in the final product increases with increasing TiC proportion in the reactant mixture. Moreover, both Ti_6Sn_5 and carbon are noticeably reduced. This implies an improvement in the evolution of Ti_2SnC by adopting TiC-containing samples. In this study, the optimum yield was achieved by the powder compact with 17.6 mol% of TiC and the corresponding XRD pattern is presented in Fig. 5(d), which shows that Ti_2SnC is the dominant phase, two impurities TiC and Sn are trivial, and Ti_6Sn_5 is no longer present. The existence of traces of TiC and Sn along with Ti_2SnC is consistent with that observed in previous studies [10–12].

According to the reaction mechanism proposed for reaction synthesis in the Ti–Sn–C system [6,11], the Ti–Sn intermetallic Ti_6Sn_5 is the first phase formed, followed by appearance of Ti_5Sn_3 from the reaction of Ti_6Sn_5 with Ti. Subsequently, Ti_2SnC is produced through interaction between Ti_5Sn_3 and TiC. In addition, the direct reaction of Ti_6Sn_5 with TiC was considered as an alternative route for the formation of Ti_2SnC [12]. The above two reaction paths are expressed in the reactions (2) and (3) regarding two different Ti–Sn intermetallics.

$$Ti_5Sn_3 + 5TiC + 2Sn \rightarrow 5Ti_2SnC \quad (2)$$

$$Ti_6Sn_5 + 6TiC + Sn \rightarrow 6Ti_2SnC \quad (3)$$

In view of the product composition presented in Fig. 5, reaction (3) is more likely for the formation of Ti_2SnC through combustion synthesis conducted in this study. Therefore, a large amount of

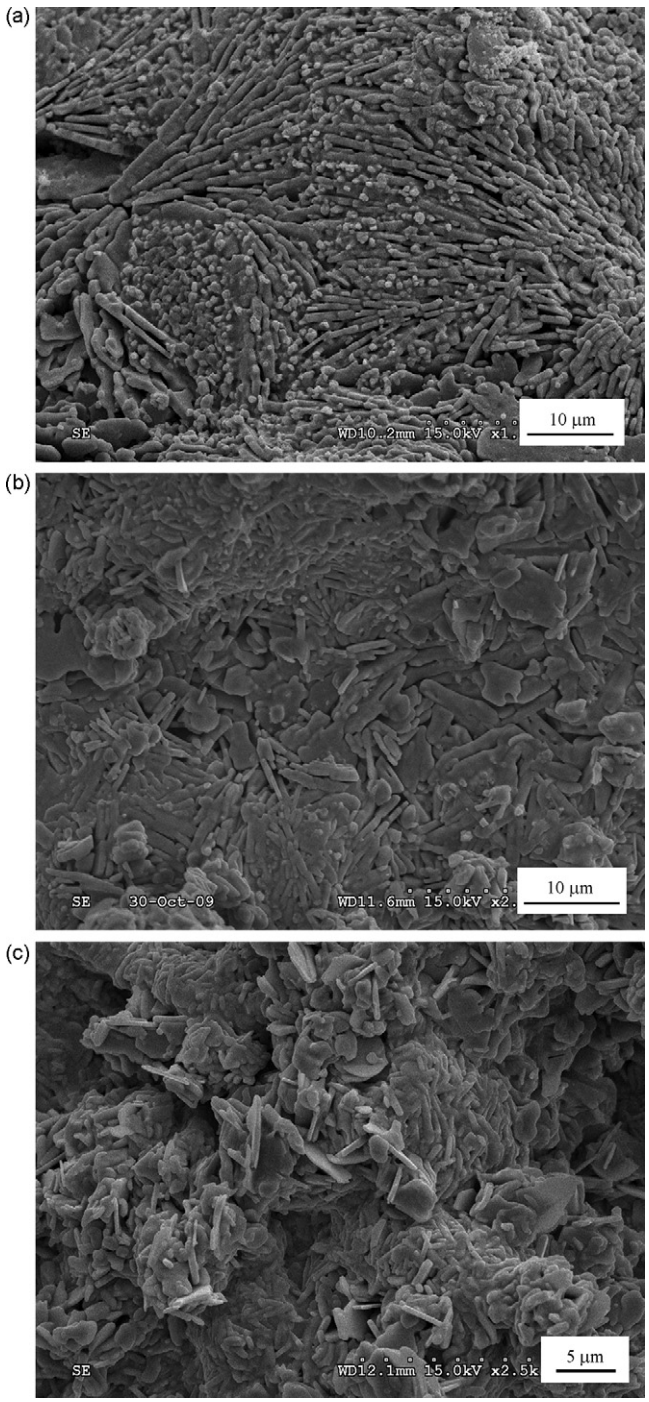

Fig. 6. SEM micrographs showing fracture surfaces of products synthesized from powder compacts of $(2-x)$Ti + Sn + $(1-x)$C + xTiC with (a) $x = 0$, (b) $x = 0.3$, and (c) $x = 0.6$.

Ti_6Sn_5 detected in the final product of the elemental powder compact is indicative of an incomplete conversion, which is probably caused by the lack of sufficient reaction time due to rapid propagation of the reaction front in the SHS process. When TiC was introduced into the reactant mixture, as shown in Figs. 3 and 4, the combustion front velocity and reaction temperature decreased significantly. A slower reaction front means longer reaction time for the evolution of product phases. The decrease of reaction temperatures from 1650 to 1190 °C is also highly beneficial to stabilize Ti_2SnC, because Ti_2SnC tends to decompose at temperatures higher than 1250 °C [11]. This well explains the improvement of Ti_2SnC

formation by the TiC-added samples and justifies the optimum yield of Ti_2SnC attained from the sample diluted with 17.6 mol% of TiC, which provides the most appropriate temperature (about 1190 °C) for stable formation of Ti_2SnC.

For the product synthesized from the elemental powder compact, Fig. 6(a) illustrates the typical microstructure of the fracture surface. It is evident that Ti_2SnC grains are in the shape of long rods with thickness of about 0.8 μm and length in the range of 6–12 μm. In addition, there are a number of small Ti_6Sn_5 particles present in Fig. 6(a). For the TiC-added sample with 8.1 mol% TiC ($x = 0.3$), Fig. 6(b) indicates that Ti_2SnC platelets appear in addition to rod-like grains and the amount of Ti_6Sn_5 granules is noticeably reduced. The addition of TiC in the reactant compact was found to favor the growth of plate-like Ti_2SnC. According to the SEM micrograph of Fig. 6(c), the Ti_2SnC platelets with a size less than 4 μm dominates in the final product of a 17.6 mol% TiC-added sample. A bimodal microstructure with rod- and plate-like grains was observed for Ti_2SnC by Li et al. [11,12]. They obtained rod-like Ti_2SnC from the Ti–Sn–C powder mixture, but plate-like Ti_2SnC from the Ti–Sn–TiC sample. Based upon the study of Li et al. [11], the growth environment with sufficient liquid phases is one of the reasons that benefits Ti_2SnC to develop a rod-like microstructure. Therefore, it is believed in this study that the decrease of reaction temperature by adding TiC in the reactant mixture reduces the amount of molten compounds in the synthesis sequence, which favors the growth of Ti_2SnC in the form of platelets instead of rods.

4. Conclusions

Preparation of the ternary carbide Ti_2SnC was conducted by combustion synthesis in the SHS mode from the elemental powder compact and TiC-added samples with TiC contents ranging from 2.6 to 17.6 mol%. For the elemental powder compacts of Ti:Sn:C = 2:1:1, the combustion front nearly 1650 °C propagates at 8.2 mm/s in a self-sustaining manner. However, due to lack of sufficient reaction time, the phase conversion was incomplete and the resultant product was dominated by the intermediate Ti_6Sn_5 rather than Ti_2SnC. The as-synthesized Ti_2SnC grains are in the shape of long rods with a length of 6–12 μm and thickness about 0.8 μm. In addition, the final products contain TiC and unreacted Sn and carbon.

For the TiC-added samples, the reaction exothermicity decreases with increasing content of TiC due to its dilution effect on combustion, thus resulting in the decrease of the reaction temperature and combustion front velocity. The reduction of reaction exothermicity was also responsible for the change in combustion behavior from the longitudinal spreading of a planar combustion front to spinning propagation of localized reaction zones when the TiC content reached 15.3 and 17.6 mol%, beyond which combustion was quenched. The slower reaction front of the TiC-added sample provides longer reaction time to achieve a better phase conversion. The lower reaction temperature is also beneficial to stabilize Ti_2SnC. As a result, the yield of Ti_2SnC was substantially enhanced by increasing TiC in the reactant mixture. In this study, the product with an optimum composition consisting of Ti_2SnC along with traces of TiC and Sn was obtained from the sample with 17.6 mol% of TiC. Moreover, the Ti_2SnC grains with a plate-like microstructure prevail in the final products of the TiC-added samples, because of the growth environment containing a lesser amount of molten compounds.

Acknowledgement

This research was sponsored by the National Science Council of Taiwan, ROC, under the grant of NSC 98-2221-E-035-065-MY2.

References

[1] M.W. Barsoum, Prog. Solid State Chem. 28 (2000) 201–281.
[2] M.W. Barsoum, D. Brodkin, T. El-Raghy, Scr. Mater. 36 (5) (1997) 535–541.
[3] W. Jeitschko, H. Nowotny, F. Benesovsky, Monatsh. Chem. 94 (4) (1963) 672–676.
[4] M.W. Barsoum, G. Yaroschuk, S. Tyagi, Scr. Mater. 37 (10) (1997) 1583–1591.
[5] T. El-Raghy, S. Chakraborty, M.W. Barsoum, J. Eur. Ceram. Soc. 20 (2000) 2619–2625.
[6] Y. Zhou, H. Dong, X. Wang, C. Yan, Mat. Res. Innovat. 6 (2002) 219–225.
[7] J.Y. Wu, Y.C. Zhou, C.K. Yan, Z. Metallkd. 96 (8) (2005) 847–852.
[8] J. Zhang, B. Liu, J.Y. Wang, Y.C. Zhou, J. Mater. Res. 24 (1) (2009) 39–49.
[9] H. Vincent, C. Vincent, B.F. Mentzen, S. Pastor, J. Bouix, Mater. Sci. Eng. A256 (1998) 83–91.
[10] H.Y. Dong, C.K. Yan, S.Q. Chen, Y.C. Zhou, J. Mater. Chem. 11 (2001) 1402–1407.
[11] S.B. Li, G.P. Bei, H.X. Zhai, Y. Zhou, J. Am. Ceram. Soc. 89 (12) (2006) 3617–3623.
[12] S.B. Li, G.P. Bei, H.X. Zhai, Y. Zhou, Mater. Lett. 60 (2006) 3530–3532.
[13] S.B. Li, G.P. Bei, H.X. Zhai, Y. Zhou, C.W. Li, Mater. Sci. Eng. A457 (2007) 282–286.
[14] Z.A. Munir, U. Anselmi-Tamburini, Mater. Sci. Rep. 3 (1989) 277–365.
[15] A. Varma, J.P. Lebrat, Chem. Eng. Sci. 47 (1992) 2179–2194.
[16] A.G. Merzhanov, J. Mater. Process. Technol. 56 (1996) 222–241.
[17] C.L. Yeh, Y.G. Shen, J. Alloys Compd. 458 (2008) 286–291.
[18] C.L. Yeh, Y.G. Shen, J. Alloys Compd. 461 (2008) 654–660.
[19] C.L. Yeh, Y.G. Shen, J. Alloys Compd. 466 (2008) 308–313.
[20] C.L. Yeh, Y.G. Shen, J. Alloys Compd. 473 (2009) 408–413.
[21] C.L. Yeh, Y.G. Shen, J. Alloys Compd. 470 (2009) 424–428.
[22] C.L. Yeh, C.W. Kuo, Y.C. Chu, J. Alloys Compd. 494 (2010) 132–136.
[23] C.L. Yeh, Y.G. Shen, J. Alloys Compd. 482 (2009) 219–223.
[24] C.L. Yeh, C.W. Kuo, J. Alloys Compd. (2010), doi:10.1016/j.jallcom.2010.02.113.
[25] C.L. Yeh, W.Y. Sung, J. Alloys Compd. 384 (2004) 181–191.
[26] C.L. Yeh, Y.L. Chen, J. Alloys Compd. 478 (2009) 163–167.
[27] T.P. Ivleva, A.G. Merzhanov, Dokl. Phys. 45 (2000) 136–141.
[28] G. Liu, K. Chen, H. Zhou, J. Guo, K. Ren, J.M.F. Ferreira, Mater. Lett. 61 (2007) 779–784.
[29] T.B. Massalski, H. Okamoto, P.R. Subramanian, L. Kacprzak (Eds.), Binary Alloy Phase Diagrams, ASM International Materials Park, OH, USA, 1996.